

## Research papers

# Multimachine stability improvement with hybrid renewable energy systems using a superconducting magnetic energy storage in power systems

V. Vishnuvardhan Yadav, B. Saravanan\*

VIT University, Vellore 632014, Tamilnadu, India



## ARTICLE INFO

## Keywords:

Multimachine power system  
Hybrid renewable energy systems  
Transient stability  
Model predictive controller  
Superconducting magnetic energy storage (SMES)  
PMSG wind turbine  
Solar PV

## ABSTRACT

Energy storage systems (ESS) have played a vital role in modern power systems to improve system stability and reliability in recent years. This paper describes the role of SMES in improving the power system stability of a multimachine interconnected with hybrid renewable energy systems (RES) such as wind and solar PV. It studies the transient stability of the system by creating a symmetrical fault in a multimachine system at various locations. The hybrid RES simulates an equivalent aggregated 75 MW photovoltaic array and a wind turbine with a capacity of 300 MW PMSG (permanent magnet synchronous generator). It couples a common DC link via a voltage source and dc/dc boost converters. A voltage source inverter connected with a step-up transformer and transmission line coupled to a multimachine system. The voltage source converter and inverter use a model predictive controller (MPC) for a better output voltage profile and to improve the system stability. A SMES is connected through a dc/dc converter with PID-SDC (Proportional Integrating Derivative Supplementary Damping Controller). It effectively suppresses power oscillations and smoothening during generation fluctuations. It reduces the low-frequency oscillations at the multimachine side during three-phase fault conditions at various locations in the system. The system's stability is improved by 3.36 s after clearing the fault. The effectiveness of the entire system is studied in the time domain simulations using MATLAB/SIMULINK software.

## 1. Introduction

In modern power system networks, hybrid RES's role has rapidly increased in the recent decade. Most of the research studies focused on hybrid RES integration into the grid. The RES has more fluctuations & unreliable based on climatic conditions, and to avoid these fluctuations & for smooth operations in modern power systems. It uses energy storage devices such as SMES (superconducting magnetic energy storage), SC (supercapacitor), BESS (Battery energy storage systems), Fuel cells etc. Wind and solar PV are the most commonly used combinations in hybrid RES [1–3].

Recently published papers explain hybrid wind-solar PV system generation technologies, control schemes, power management strategies, and stability analysis [1–5]. In [4], proposed standalone applications of hybrid power generation consist of wind, solar PV, battery, and fuel cell. In that scheme, primary sources are wind and solar PV. The other secondary sources are batteries and fuel cell used as long-term storage and backup.

In [5], it proposes the design and sizing of hybrid wind-solar PV

methodologies and control schemes. In [6] it suggests a current injecting method for grid synchronization of wind farms during severe grid faults. In [7] it proposes a BESS (battery energy storage system) to enhance the multimachine power system's transient stability and frequency stability for better transient performance during temporary and permanent faults. It proposes PI lead and PI lead-lag control schemes. In hybrid wind-PV power generation systems with grid connection, it uses a genetic multi-objective algorithm and appropriate sizing in order to optimize autonomous wind-PV eco-design and a hybrid wind-PV-battery power-generation system with grid integration, even though the strategy is on distinct optimization methods with multi-criteria decision analysis is presented in [8]. In [9] to improve the dynamic and transient stability of the connected SG, In the controlling block of DFIG, it suggests a novel control scheme “transient controller (TC),” “electromagnetic torque band damping controller (ETBDC),” and “reactive power band damping controller (RPBDC),” to adjust the controller parameters it uses genetic algorithms. It presents a wide area of control to improve the transient stability of wind farms and synchronous generators [10]. Neural Networks (NNs) and Reinforcement Learning (RL) methods proposed a new

\* Corresponding author.

E-mail addresses: [vishnuvardhan.v@vit.ac.in](mailto:vishnuvardhan.v@vit.ac.in) (V.V. Yadav), [bsaravanan@vit.ac.in](mailto:bsaravanan@vit.ac.in) (B. Saravanan).

<https://doi.org/10.1016/j.est.2022.106255>

Received 1 September 2022; Received in revised form 17 November 2022; Accepted 25 November 2022

Available online 7 December 2022

2352-152X/© 2022 Elsevier Ltd. All rights reserved.

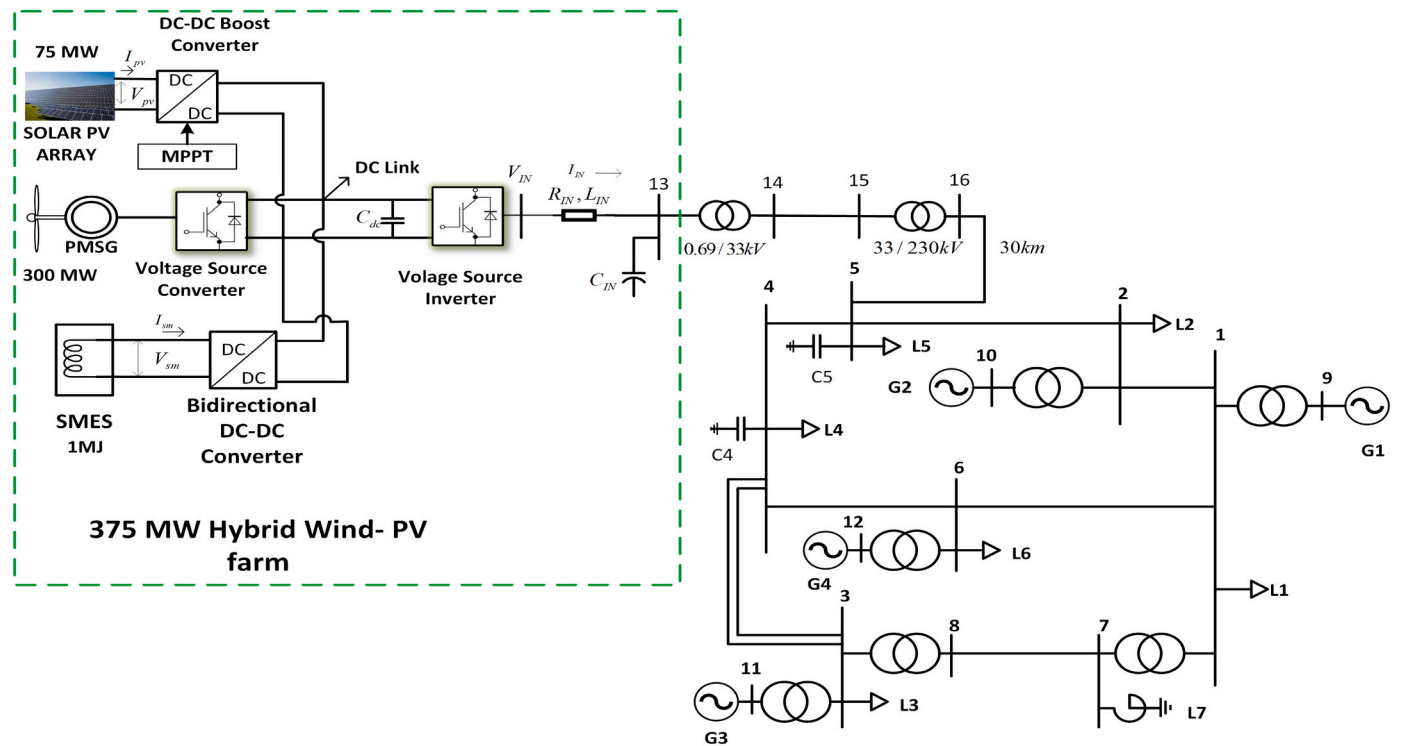


Fig. 1. Configuration of the large-scale hybrid RES connected with the studied multimachine system through a proposed SMES-based ESS.

algorithm of nonlinear optimal control. Several grid-integrated hybrid PV-wind power management strategies were presented in [11–13]. In [11] It discusses a hybrid power-generation system grid-connected with a Wind turbine, PV array, and flywheel energy-storage technology. The proposed technique provides a cost-effective hybrid power supply to choose the most suitable control method for grid-connected home applications. In [12] developed and validated a novel energy-management system based on an adaptive neuro-fuzzy system inference for a grid-integrated hybrid power system including a Wind turbine, solar PV, hydrogen, and battery-based energy storage system. In [13] a new power-management method was proposed for a dc microgrid integrating hybrid RES consisting of solar PV, wind with batteries, and SC.

In recent years the SMES technologies are widely used in various power system applications to enhance the system performance. In [14], mentioned various energy storage systems employed in power system applications. In that, SMES suits for high power grid support systems, among other energy storage devices. In [15] SMES is highly efficient at transferring electrical power with the grid in response to small and large disturbances due to its dynamic characteristics. SMES plays a vital role in integrating renewable energy sources into the grid, improving system stability, and controlling the wind turbine's output power. In [16] battery & SMES-based DVR ("dynamic voltage restorer") is used to compensate for the voltage sag condition in hybrid RES consisting of wind and solar PV. An MW range, SMES-based DVR, and SFCL ("superconducting fault current limiter") are proposed to compensate for the voltage sag [17], 0.3H/1.76kA SMES is designed for MW range power operations.

In [18] SMES and battery-based hybrid energy storage system is designed to reduce grid voltage fluctuations. To control the SMES, "DC bus voltage signalling" and "voltage droop control" methods are used. In [19] a STATCOM (a synchronous compensator) with BESS is proposed to reduce the SSR (sub-synchronous resonance) in a wind farm tied with a weak grid. A STATCOM/BESS is connected in parallel with the grid to reduce the SSR, and a grid stiffness control strategy is used to control STATCOM/BESS. A UPFC ("unified power-flow controller") is proposed to reduce the SSR in hybrid power generation coupled with an infinite

bus via a compensated line consisting of a series capacitor [20]. That hybrid generation is consisting a steam turbine generator and an offshore wind farm. A damping controller has been proposed for UPFC, and it reduces low-frequency oscillations.

A SMES with a fuzzy controller is proposed to enhance the performance and analyse the fault ride through of DFIG fed to a weak grid. A hysteresis current controller is designed to perform the VSC switching operations for SMES. A fuzzy controller is proposed for the DC-DC chopper to exchange the energy between the integrated system and SMES [21]. In [22] a new eve-triggered control method is proposed for SMES to improve the microgrid's voltage stability and frequency stability. The microgrid stability is analysed by considering two cases. In the first case, unplanned disconnection of supply units in the microgrid and studied the system stability during this period, SMES gives backup immediately, and the system gets stable in 4 s. In the second case, high power load switching at  $t = 3.5$  to  $t = 4.5$  s. During this, SMES successfully handle to improve the system stability. In [23] SMES and TCSC ("Thyristor controlled series capacitor") applications are analysed for improving the load frequency control in the HVDC tie link. In the HVDC system, two areas of AGC("Automatic Generation Control") dynamic performance of thermal-thermal and hydro-thermal power systems with and without SMES TCSC analysed, with SMES and TCSC improves the settling time of the system. A new optimized reactive power dispatch method is proposed for the hybrid RES PV with SMES connected to the grid. It improves the converter efficiency in both PV and SMES sections. Two algorithms were proposed for active and reactive power control in both PV and SMES converters. They analysed the system performance during fixed and variable load conditions [24].

In grid-connected PV systems with SMES, the SMES converter's digital control delay is proposed to enhance the system's stability. SMES digital control delay  $T_{dm}$  varies from 0 to 300  $\mu$ s based on this operating frequency, and the SMES converter is chosen for switching [25]. To find the online power system stability with the eigenvalues method, a 1 MJ mobile SMES is used. The SMES is designed with MgB2 Rutherford cables with cryocoolers. The eigenvalue analysis method uses to identify the optimal location for SMES in the system and moved to that location

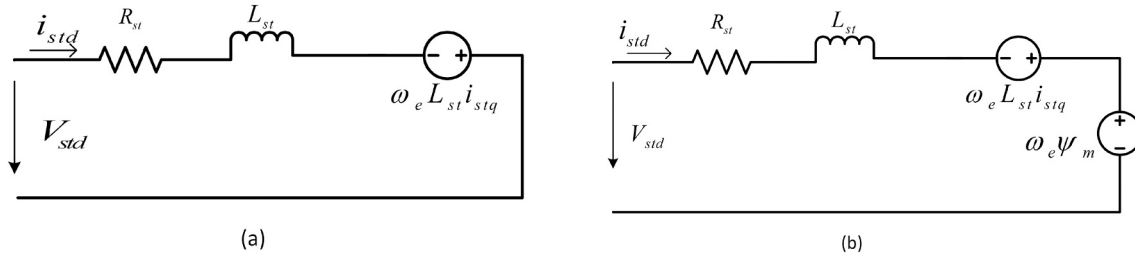


Fig. 2. PMSG equivalent circuit (a) d-axis (b) q-axis.

to improve the stability [26]. In a DC microgrid, SMES is utilized for power regulation with a voltage-based segmented control technique during the transient period to improve the system performance [27]. The voltage-based segmented control is designed based on DBS (“DC bus signaling”). It allows the SMES to perform stable operations without any communications in the DC Microgrid. The voltage-based segmented control facilitates the SMES. During DC voltage variations, it regulates the spontaneous power of the DC Microgrid.

In the papers, as mentioned earlier [4–8,13] despite having relatively small capacities, it proposes hybrid power generation systems with wind-PV for standalone operation or integration into distribution systems. In contrast, Research on large-scale power generation of hybrid RES integrated into the grid is lagging. Still, multiple demonstration projects have been initiated on less MW-range hybrid power generation of wind-PV systems over the last several years. However, there are still significant obstacles to overcome. Such large-scale power generation systems of hybrid wind-PV for grid integration have received little attention. Only a few researchers are focused on large-scale hybrid power generation. In [28] paper, the authors described the stability improvement with the help of a supercapacitor in a large-scale wind PV hybrid system interconnected to a multimachine. The transient stability was determined during a three-phase fault at one particular location.

This paper presents the multimachine system stability analysis of interconnected 375 MW hybrid wind and solar PV systems with SMES energy storage unit. A model predictive controller (MPC) is replaced instead of the traditional PI controller in VSC and VSI to improve the system stability and voltage profile. Here the stability was analysed during faults at various locations in the multimachine system and compared with previous results. SMES energy storage unit smoothes power fluctuations during wind speeds and solar irradiation variations. PID-SDC (Proportional Integrating Derivative Supplementary Damping Controller) was designed to reduce low-frequency oscillations to improve stability.

In the above literature, many researchers have studied the power system stability improvement with different energy storage systems in recent years. Among all the energy storage devices, SMES has more advantages in handling the high-power rating applications in modern power systems. There is still a research gap in investigating new methods to improve power system stability in hybrid RES. The primary motivation of this work is to present the challenges in the study and improve the stability issues in grid-integrated large-scale hybrid renewable energy systems with an energy storage device and robust controllers.

This paper organizes as follows. Section 2 presents the configuration and mathematical models used for the analysed system. Section 3 describes the system’s control schemes, Section 4 represents the simulation analysis, and Section 5 concludes the paper.

## 2. Configuration of the system

Fig. 1 represents the complete structure of the multimachine system interconnected with a 375 MW hybrid with the proposed SMES energy storage device. Here the 375-MW hybrid wind-solar PV farm consists of

150 units, each of 2 MW wind and 0.5 MW of PV, a 300-MW PMSG-based wind, and a 75-MW solar PV array. The wind-solar PV system couples to a common DC link along a voltage source converter (VSC) and dc/dc boost converter with MPPT. The multimachine system is connected by a common DC link at any of the buses through a voltage source inverter. That converts DC to AC, step-up transformers, and a transmission line length of 30 Km. The PV array is a dc/dc boost converter along with the MPPT function for getting better efficiency. The dc link power gets fluctuations because their input power sources of wind and solar PV get variations due to changes in wind speeds and solar irradiations. An energy storage system based on SMES is placed for smoothing the power fluctuations. The multimachine consists of four synchronous generators interconnected with each other with different types of loads. The detailed description is mentioned in [29,30].

### 2.1. Mathematical modelling of wind turbine

The wind turbine’s mechanical power output can be written by

$$P_m = \frac{1}{2} \rho_w A_t C_{pwi}(\lambda_t, \beta_t) V_w^3 \quad (1)$$

Here  $\rho_w$  is the air density in  $\text{Kg/m}^3$ ,  $A_t$  is the swept area of turbine blades ( $\pi R_t^2$ ),  $C_{pwi}$  is the wind turbine’s power coefficient, which is the product of tip speed ratio  $\lambda_t$  and pitch angle  $\beta_t$ , [31,32]. The tip speed ratio is represented as

$$\text{Tip speed ratio } \lambda_t = \frac{\omega_s R_t}{V_w} \quad (2)$$

Here  $\omega_s$  is the rotational speed of the turbine rotor in rad/s,  $R_t$  which is the radius of the turbine. In the modelling of the wind turbine’s power coefficient can be expressed as follows

$$C_{pwi} = c_1 \left[ c_2 \psi - c_3 \beta_t - c_4 \beta_t^{c_5} - c_6 \right] e^{-\frac{c_7}{\psi}} \quad (3)$$

Here

$$\frac{1}{\psi} = \left[ \frac{1}{\lambda_t + c_8 \beta_t} - \frac{c_9}{1 + \beta_t^3} \right] \quad (4)$$

Here  $c_1 - c_9$  are the coefficient constants  $\lambda_t$  is the tip speed ratio and  $\beta_t$  is the pitch angle.

### 2.2. Modelling of PMSG

Fig. 2 represents the equivalent circuit to design a mathematical model of the PMSG in the dq axis frame.

The stator equations of the voltage at the d-axis are  $V_{std}$ , and at the q-axis  $V_{stq}$  can be expressed as

$$V_{std} = R_{st} i_{std} + L_{st} \frac{di_{std}}{dt} - \omega_e L_{st} i_{stq} \quad (5)$$

$$V_{stq} = R_{st} i_{stq} + L_{st} \frac{di_{stq}}{dt} + \omega_e L_{st} i_{std} + \omega_e \psi_m \quad (6)$$

Here  $R_{st}$  is stator resistance,  $L_{st}$  is the stator inductance,  $i_{std}, i_{stq}$  are the

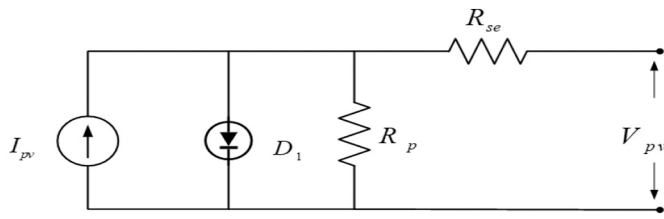


Fig. 3. Single diode model of PV cell equivalent circuit.

stator currents in dq-axes,  $\omega_e$  the PMSG angular frequency, and  $\psi_m$  is the PMSG rotor flux linkage [33].

2.3. Modelling of PV array with dc-dc boost converter

Fig. 3 represents the equivalent circuit of the single diode model of PV cell. From [34–36] PV array is designed by using methods proposed in [35,36] PV array output current ( $I_{pv}$ ) can be expressed as

$$I_{pv} = N_p I_{Sp} - N_p I_0 \left\{ \exp \left( q(V_{pv} + R_{Ase} I_{pv}) / kATN_{se} N_s \right) - 1 \right\} - (V_{pv} + R_{Ase} I_{pv}) / R_{Ap} \tag{7}$$

Here  $N_p$ ,  $N_s$  are the number of connected PV modules in parallel and series in an array.  $I_{Sp}$  is the PV cell current,  $I_0$  is reverse saturation current,  $N_{se}$  is the number of cells connected in a PV module,  $V_{pv}$  is the PV array output voltage in volts,  $R_{Ase}$ ,  $R_{Ap}$  are the PV array series, and

parallel equivalent resistance in Ohms,  $q$  is an electron charge respectively,  $k$ ,  $A$  are the constants. The expressions of  $I_{Sp}$  and  $I_0$  mentioned in [34–37].

Fig. 4 represents the dc/dc boost converter simplified representation connected from the PV array to the common DC link. The mathematical equations of the dc/dc boost converter are represented in [37].

2.4. Modelling of SMES and DC-DC converter

The superconducting materials are the essential aspect of the SMES system. These materials do not experience any dissipation in the system because there is no resistance to these materials. These materials are used to make the coil to reduce the amount of energy lost due to conductivity. The magnetic field is capable of storing a significant amount of energy. The coil is in a superconducting state, in which the cryogenic system can respond effectively and in which there is a protective mechanism to secure the SMES under rare conditions, which is the most challenging problem that the SMES unit faces. Controlling the electronic converter circuits allows for the impedances between the SMES coil and

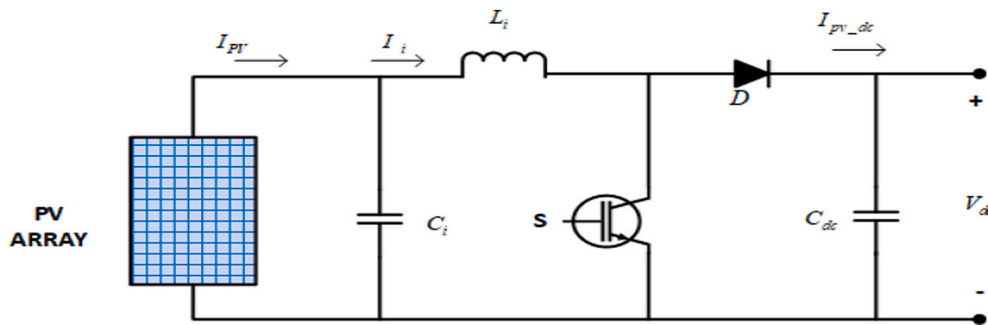


Fig. 4. Simplified representation of the dc-dc boost converter.

the grid. Eq. (8) represents the power and energy of the SMES.

$$E_{sm} = \frac{1}{2} L_{sm} i_{sm}^2 \tag{8}$$

Here  $E_{sm}$  represents the energy of the SMES,  $L_{sm}$  which is the inductance of the coil,  $i_{sm}$  is current, and  $V_{sm}$  represents the voltage of the

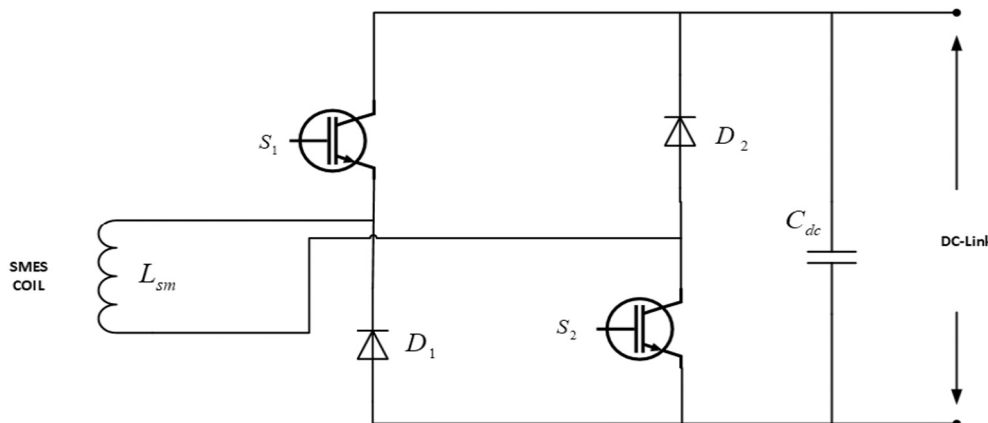


Fig. 5. The bidirectional dc-dc converter fed to SMES.

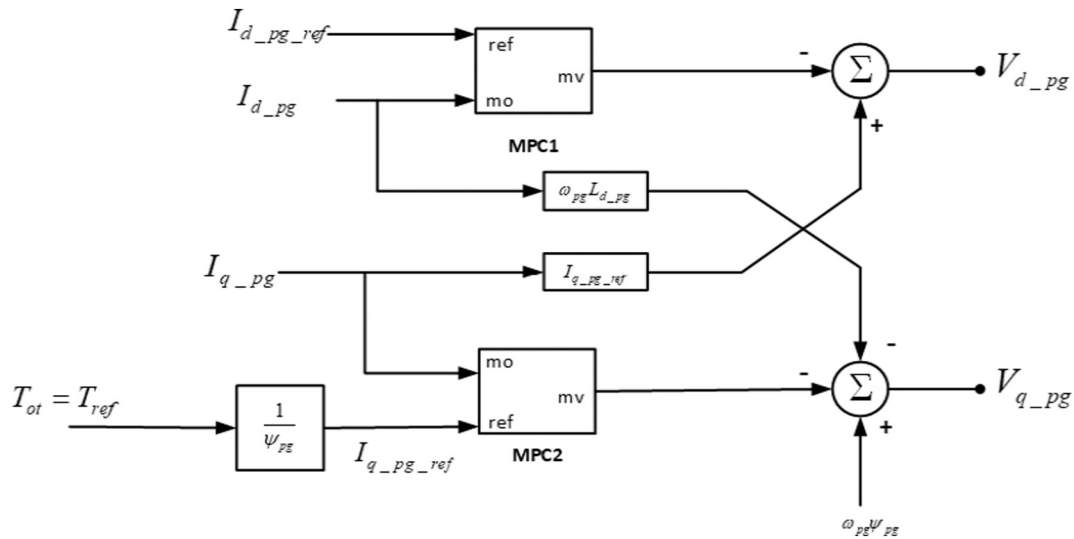


Fig. 6. Schematic control diagram of VSC for PMSG.

SMES.

$$P_{sm} = \frac{dE_{sm}}{dt} = L_{sm} i_{sm} \frac{di_{sm}}{dt} \tag{9}$$

$$P_{sm} = V_{sm} \cdot i_{sm} \tag{10}$$

The bidirectional dc-dc converter, fed to SMES and the common dc link, has two switches,  $S_1$  and  $S_2$ , and diodes  $D_1$  and  $D_2$ , as shown in Fig. 5.

The bidirectional dc-dc converter interconnects in this simulation between SMES and the common dc link. The switching of  $S_1$  and  $S_2$  does appropriately neglected, simulating the dynamic average value method mentioned in [38]. The parameters for SMES are stored energy is 1MJ, the critical current is 565A, inductance is 6.28H, and DC link

capacitance is 0.12F.

### 2.5. The model of VSI with LC filter

The voltage source inverter (VSI) is connected between common dc link and the point of common coupling (PCC). The VSI connects to a 0.69/33 kV step-up transformer and then to a 33/230 KV transformer through a transmission line. The 33/230 KV transformer is connected to the multimachine system through a transmission line of length is 30 km. The LC filter is designed to reduce the output voltage ripples in the VSI. The LC filter differential equations of in dq-axes frame represented in p.u are referred to in [28]. The multimachine design and mathematical models are referred from [29,30,39].

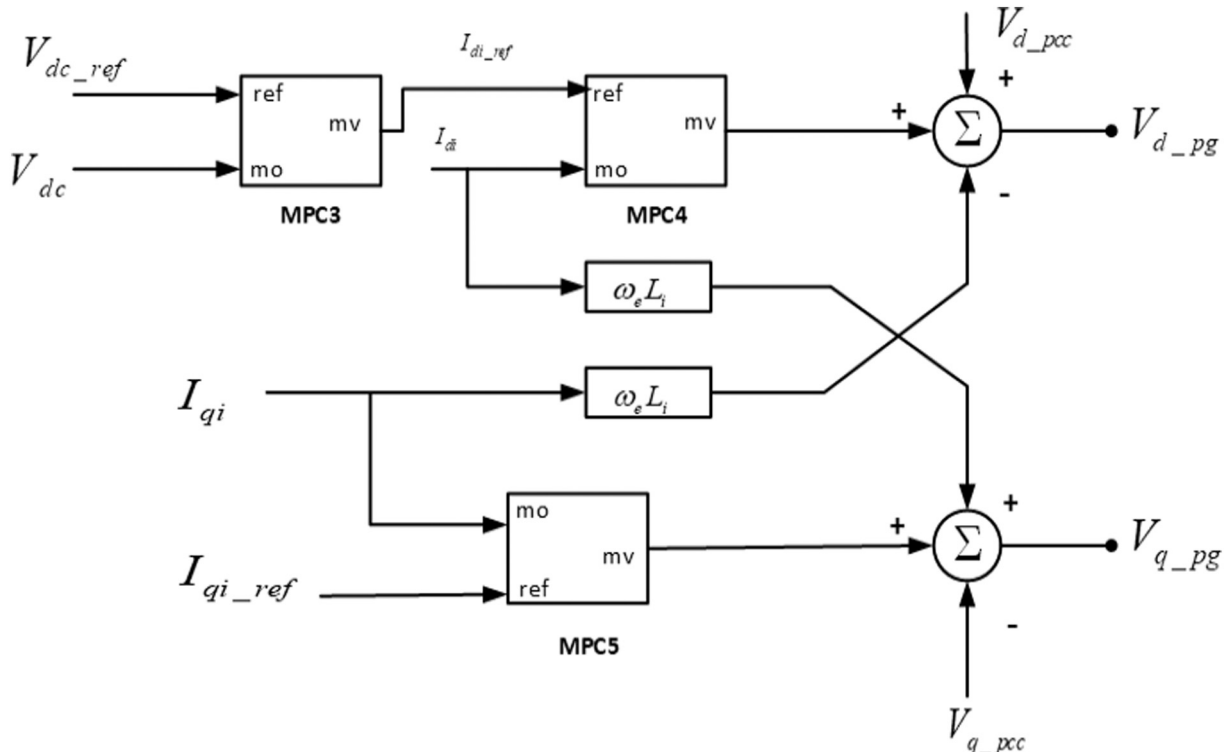


Fig. 7. Schematic control diagram of VSI.

### 3. Control schemes of the system

#### 3.1. Control of PV array's dc/dc boost converter

In a PV array, maximum power point tracking (MPPT) is essential to get maximum efficiency. An MPPT control scheme proposes to control the dc-dc boost converter using the traditional perturbation and observation (P&O) algorithm. The detailed principle of perturbation and observation (P&O) MPPT algorithm can be obtained from [39,40].

#### 3.2. Control of wind PMSG's voltage source converter

The schematic control block diagram of VSC for PMSG is shown in Fig. 6. The main aim of this converter is to get the maximum power of the wind PMSG. In order to meet this, the optimal control torque method is applied [31]. In this method, by measuring the wind PMSG rotor speed, the optimal torque is obtained by using Eq. (11).

$$T_{ot} = k_{ot}\omega_{pmsg}^2 \quad (11)$$

Here  $k_{ot}$  is a constant which is determined from wind turbine characteristics. A model predictive controller (MPC) is used in this torque control method of PMSG. The control method is straightforward, and it consists of reference currents, a predictive model, and the cost function minimization method mentioned in [41]. Torque is controlled by the current of the d-axis in PMSG to minimize power loss. The d-axis current is taken as a reference and is equal to zero.

#### 3.3. Control method of voltage source inverter

Fig. 7 shows the control scheme of the voltage source inverter. The VSI controller aims for the dc-link voltage  $V_{DC}$  to be kept at a reference value of  $V_{DC,R}$  and to regulate the VSI's reactive power transfer to the ac grid. The control scheme of the VSI is done in the dq-axis reference frame with a model predictive controller [41] with the voltage vector of the PCC aligned with the d-axis, to achieve decoupled control of the active and reactive components. Thus, the VSI's d- and q-axis currents control the dc-link voltage and reactive power exchanged with the ac grid. The detailed designed parameters are referred to from [42].

The predictive controller calculates the PMSG current error in  $(k+1)$  sampling instant, and the reference currents are summarized to  $(k+1)$ . The estimate equation is represented as

$$i_{dq}^*(k+1) = 2i_{dq}^*(k) - i_{dq}^*(k-1) \quad (12)$$

The predictive controller cost function minimization with current control, capacitor voltages, and frequency minimization is represented as

$$g_{in}(k) = \lambda_{ind}g_{ind}(k) + \lambda_{inq}g_{inq}(k) + \lambda_{dc}g_{dc}(k) + \lambda_{ins}g_{ins}(k) \quad (13)$$

Here  $\lambda_{ind}$ ,  $\lambda_{inq}$ ,  $\lambda_{dc}$  and  $\lambda_{ins}$  are the weighting factors of the cost functions  $g_{ind}$  and  $g_{inq}$  calculated the error in dq frame.

#### 3.4. Control of SMES-based bidirectional dc/dc converter

The bidirectional dc/dc converter uses two feedback control loops in a cascade to operate. The SMES either injecting or absorbing the active power regulates the outer loop from the common dc link. The inner control loop adjusts the SMES's current to match the reference value generated by the external control loop. The PID-SDC (Proportional Integrating Derivative Supplementary Damping Controller) proposes the bidirectional dc/dc converter for the power control loop. The main objective of this controller is to improve the multimachine power system synchronous generator's ( $P_{G1} - P_{G4}$ ) low-frequency oscillations damping characteristics. The PID-SDC (Proportional Integrating Derivative Supplementary Damping Controller) is designed based on the pole assignment method. PID-SDC uses the rotor speed difference between

**Table 1**

PSO parameters.

No. of particles	20
No. of swarms	3 ( $K_p, K_i, K_d$ )
No. iteration	1000
Search Intervals	0-500
c1, c2	2,2

generator 2 (G2) and generator (G4), which generates an additional control signal applied toward the power control loop of the bidirectional dc/dc converter to enhance damping characteristics. The detailed design of the PID-SDC (Proportional Integrating Derivative Supplementary Damping Controller) is mentioned in [42].

In this work, in order to fine tune the PID design parameters we have used PSO ("Particle Swarm Optimization") algorithm to find the optimal values. The value of  $K_p$ ,  $K_i$ , and  $K_d$  is almost nearer to the one which was found earlier using pole assignment method [42].

The value of PID design parameter with tuning of PSO algorithm is as follows

$$K_p = 57.15, K_i = 35.28, K_d = 92.85$$

The following Table 1 represents the PSO parameters.

### 4. Simulation analysis

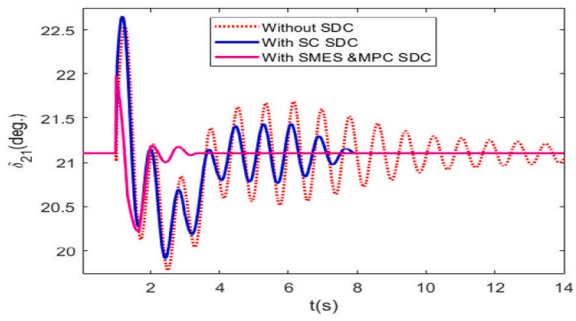
The effectiveness of the proposed Model predictive controller and SMES PID supplementary damping controller during a 3- $\phi$  short circuit fault at two different locations in the system and observed performance. The entire system is analysed in the time domain simulation analysis and simulated in MATLAB/SIMULINK software. This analysis considers three cases. In case-I, at the bus no 4 of 230 kV, a 3- $\phi$  short circuit fault is created, and the transient stability of the system is studied. In case- II, a 3- $\phi$  short circuit fault is created at the bus no 7 of voltage level 400 kV. During this condition, transient stability of the multimachine system is observed. This analysis assumes that the solar irradiance and wind speed are constant in case-I and case-II. In case- III, we studied how SMES reduces the power generation fluctuations in the hybrid RES connected with the multimachine system during variations in the solar irradiation and wind speed.

Case-I: Effectiveness of the proposed MPC, SMES &SDC to improve the transient stability during 3- $\phi$  short circuit fault at bus no 4 of 230 kV:

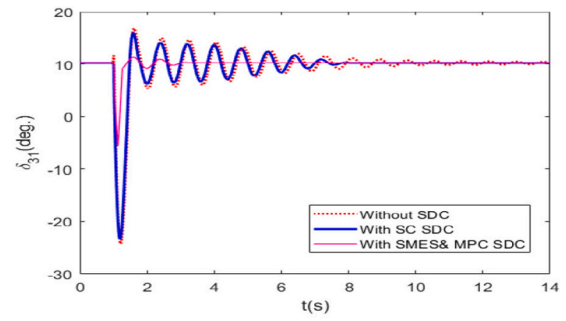
In this case, at 230 kV bus no 4, a 3- $\phi$  short circuit fault is created at  $t = 1.0$  s, cleared at  $t = 1.1$  s, and observed system stability. Fig. 8 represents the comparative plots of the system without SDC, with SC& SDC, with MPC, SMES &SDC. The existing system using the SC&SDC system is stable at 6 s after clearing the fault. With the proposed MPC, SMES &SDC, the system gets back into the stable after 3.36 s after clearing the fault. On the other hand, the low-frequency damping oscillations are quickly eliminated and improve the system's transient response. In Fig. 8(a)-(c), the plot clearly shows that the proposed controller improves the transient performance after clearing the fault the system gets back to stable very quickly. Fig. 8 (d)-(g) plots show the generator's (1-4) power variations after clearing the fault. In this condition, the wind speed and solar irradiation is assumed as constant.

Case-II: Effectiveness of the proposed MPC controller SMES &SDC to improve the transient stability during 3- $\phi$  short circuit fault at bus no 7 of 400 kV:

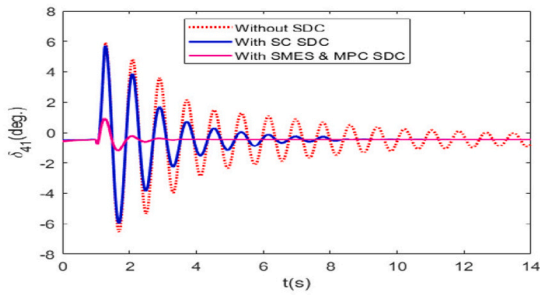
In this case, at bus no 4 of 400 kV, a 3- $\phi$  short circuit fault is applied at  $t = 1.0$  s and cleared at  $t = 1.5$  s. During this condition, the proposed MPC, SMES &SDC perform efficiently, and the system is stable at 3.45 s



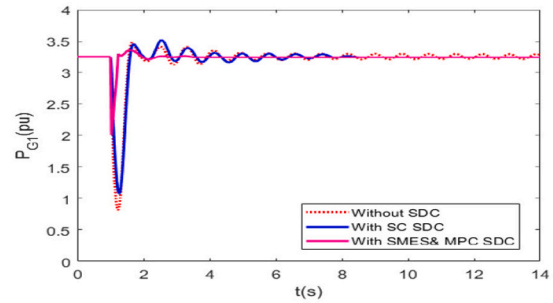
(a)



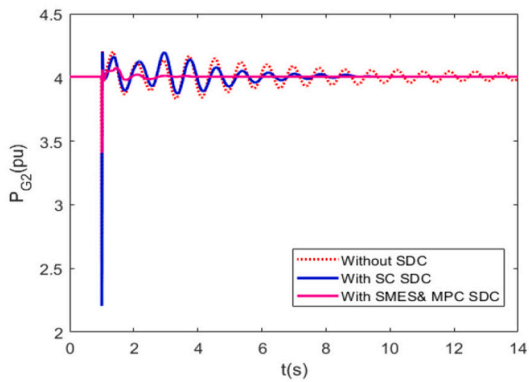
(b)



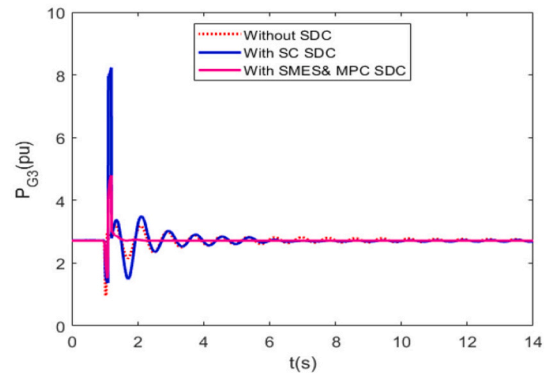
(c)



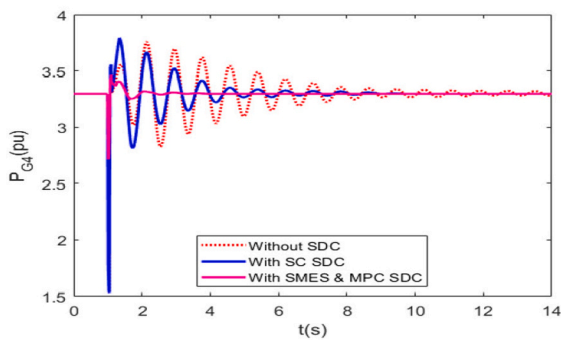
(d)



(e)

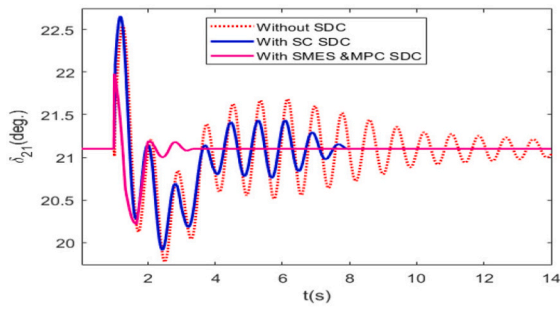


(f)

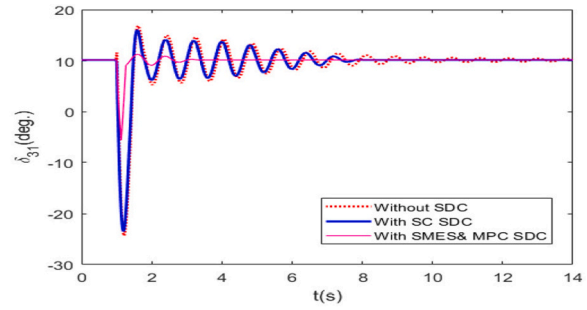


(g)

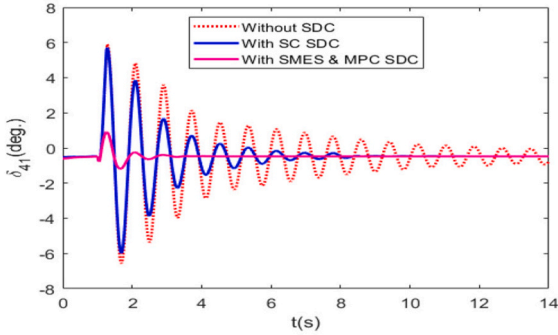
**Fig. 8.** Comparative plots of the system without SDC, with SC& SDC, with MPC controller SMES &SDC during 3- $\phi$  short circuit fault at bus 4. (a)  $\delta_{21}$ , (b)  $\delta_{31}$ , (c)  $\delta_{41}$ , (d)  $P_{G1}$ , (e)  $P_{G2}$ , (f)  $P_{G3}$ , (g)  $P_{G4}$ .



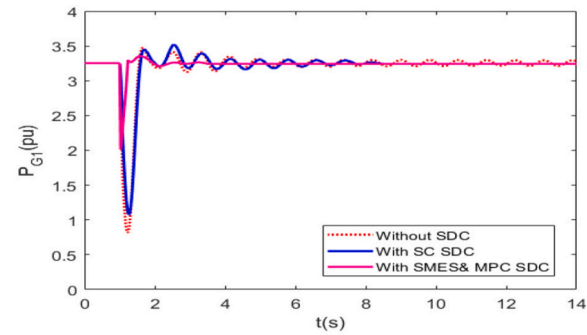
(a)



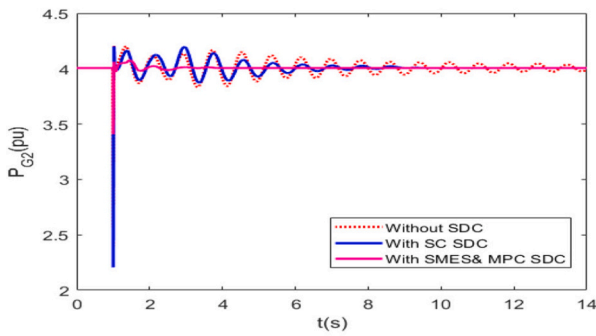
(b)



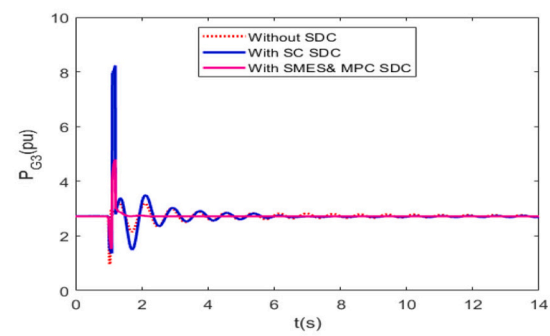
(c)



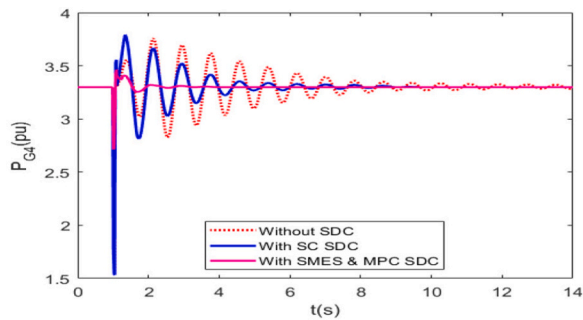
(d)



(e)



(f)



(g)

Fig. 9. Comparative plots of the system without SDC, with SC & SDC, with MPC, SMES & SDC during 3- $\phi$  short circuit fault at bus 4. (a)  $\delta_{21}$ , (b)  $\delta_{31}$ , (c)  $\delta_{41}$ , (d)  $P_{G1}$ , (e)  $P_{G2}$ , (f)  $P_{G3}$ , (g)  $P_{G4}$ .

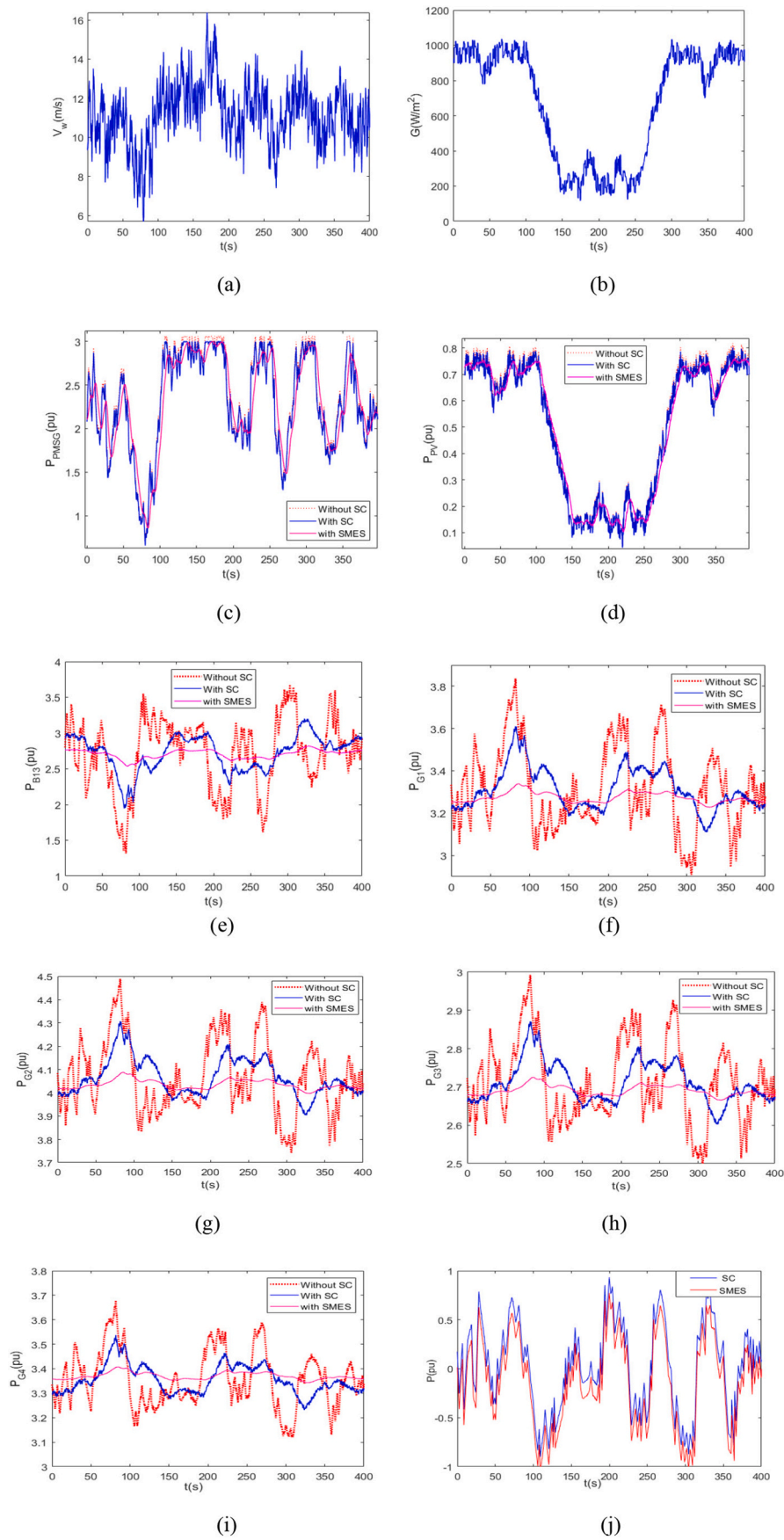


**Fig. 10.** Dynamic response during various variations of wind speed and solar irradiation of the studied system. (a) Wind speed  $V_w$  (m/s), (b) solar irradiation  $G$  ( $W/m^2$ ), (c)  $P_{PMSG}$ , (d)  $P_{pv}$ , (e)  $P_{B13}$ , (f)  $P_{G1}$ , (g)  $P_{G2}$ , (h)  $P_{G3}$ , (i)  $P_{G4}$ , (j) Comparison of SC & SMES power.

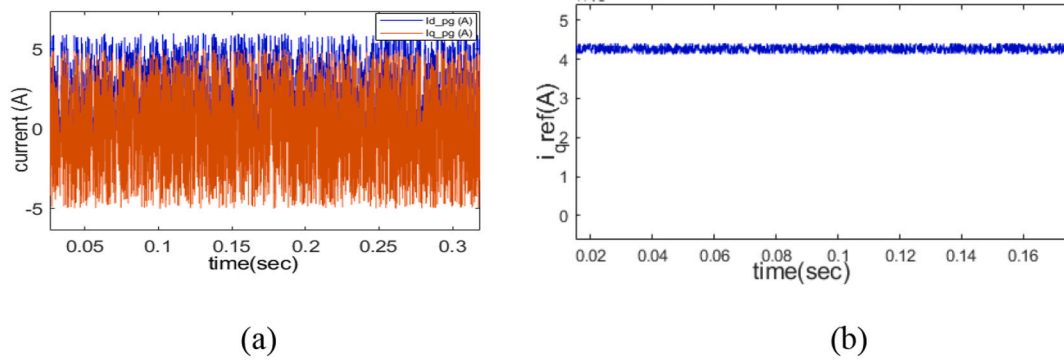


Fig. 11. Input signals for MPC for VSC (a)  $i_{d,pg}$  and  $i_{q,pg}$ . (b)  $i_{q,pg}$  ref.

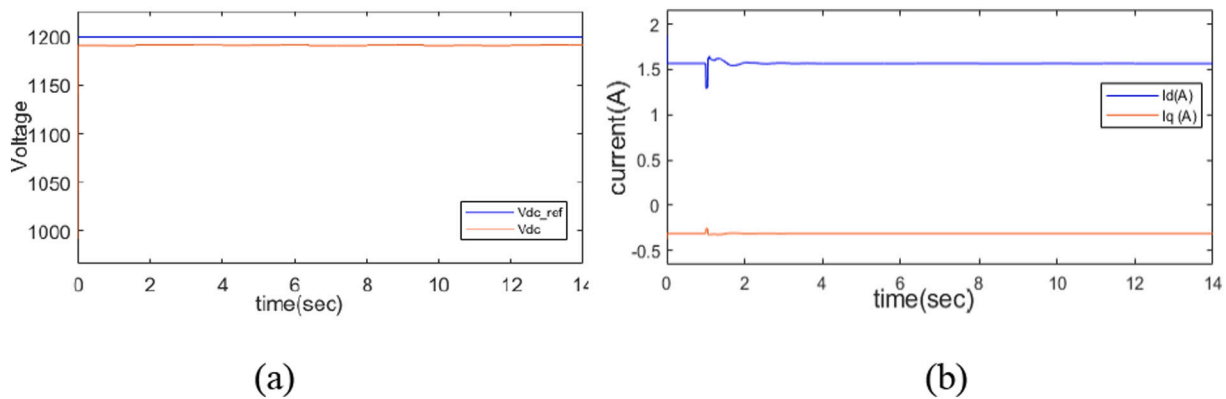


Fig. 12. Input signals for MPC for VSI (a)  $V_{dc}$  &  $V_{dc,ref}$  (b)  $i_d$  &  $i_q$  of the inverter.

after the clearance of the fault, the plots are shown in Fig. 9. During this fault, the generator1 is outage from the system, then the system stability is not affected, and the hybrid RES and other generators in the grid have compensated the load. In this case, variations in wind speed and solar irradiation is assumed as constant. Fig. 9. (a)–(c) represents the multimachine system transient response after clearing the fault condition. Fig. 9 (d)–(g) plots show the generator's (1–4) power variation curves after removing the fault. Observing the power variation, it settles down very quickly with SMES and MPC SDC compared to without SDC and SC. The main advantage in both cases, I & II, is the quick response of the controller with SMES during the fault condition and getting back to a stable condition in less time than other methods.

Case III: Effectiveness of the proposed SMES in decreasing the power generation fluctuations of hybrid RES-connected multimachine system.

In this case, the proposed SMES smoothing the power fluctuations of the multimachine power system fed to hybrid RES under various solar irradiance and wind speed is studied and compared with the existing system. Fig. 10 (a) and (b) show the variations in solar irradiance and wind speed, the real-time data of wind speed, and solar irradiances referred to [42]. A comparison of the system's dynamic behaviour under various wind and solar irradiance disturbances with and without the SC & SMES is plotted in Fig. 10 (c)–(i).

Fig. 10 (c) and (d) represent the wind PMSG and solar PV array's output power dynamic response. We can observe that as wind speed changes, the output power of wind turbines and solar arrays changes. For the examined system, with SC and with SMES, we find that wind PMSG output power dynamic responses are identical. Due to the VSC's control on the WTG, it follows its MPPT characteristic regardless of the SC & SMES that is presented. Without ESS, with SC, and with SMES, the

dynamic responses of the PV array's output power are identical, as is the PV array's output power dynamic response for both scenarios.

It is shown in Fig. 10 (e)–(i) that the dynamic responses of other essential system parameters, like Bus 13 (PB13) active power and the active powers of generators 1–4 (PG1–PG4), are comparable when the SC & SMES is present or absent. When the SMES is not in use, the examined system's dynamic responses may be seen to fluctuate significantly due to changes in wind speed and solar irradiation. The proposed SMES, on the other hand, can successfully dampen these fluctuations in the tested system.

As demonstrated in Fig. 10 (j), the comparison of SC & SMES can either inject or absorb power to adjust for these changes. As a result, it can say that the suggested SMES can reduce power fluctuations better than the SC and enhance the study system's performance when wind speed and solar irradiation vary simultaneously.

#### 4.1. Control input for MPC

In this section, the control input plots of the model predictive controller for VSC (voltage source converter), and VSI (Voltage Source Inverter) is represented in Fig. 11 (a), (b), and Fig. 12 (a)&(b). In Fig. 11 (a) illustrates the stator currents in the dq-axes frame represented as  $i_{d,pg}$  and  $i_{q,pg}$ . Fig. 11 (b) is the reference current of the stator in q axes is represented as  $i_{q,pg}$  ref. the reference current of d axes is assumed as zero. In Fig. 12 shows the input signals for the model predictive controller for VSI. The input dc voltage at the common dc link  $V_{dc}$  and the reference voltage of  $V_{dc}$  is represented in Fig. 12 (a). The inverter dq-axes currents are shown in Fig. 12 (b)

## 5. Conclusion

This paper presents the transient stability analysis results of a

multimachine power system interconnected with a large-scale hybrid RES consisting of wind-solar PV with an energy storage device. The stability of the multimachine system is analysed by considering three cases. In the first case, the 3- $\phi$  short circuit fault is created at the bus no 4 at  $t = 1$  s and cleared at  $t = 1.1$  s. During this, the system gets stable after 3.36 s. In the second case, the 3- $\phi$  short circuit fault is created at the bus no 7 at  $t = 1$  s and cleared at  $t = 1.5$  s. After clearing the fault, the system gets stable in 3.46 s. A SMES energy storage device is used and compared with the existing system results in case III. It performs more accurately than previous systems in smoothening the power fluctuations due to various solar irradiation and wind speeds. A SMES's bidirectional dc/dc converter is consisting PID-SDC. It improves the synchronous generator's low-frequency oscillations damping characteristics of the multimachine system during the 3- $\phi$  short circuit fault at various locations. A model predictive controller is proposed for VSC and VSI for a better voltage profile. Also, it improves stability by lowering oscillations along with the PID-SDC controller. Time domain simulation results show the analysed system's dynamic and transient performances under disturbance conditions. All the simulations are evaluated in MATLAB/SIMULINK. The future scope of this work will extend to study the system's dynamic stability by considering various faults simultaneously in both RES and multimachine systems. We can also include the controllers like artificial intelligence, robust controllers etc. to analyse the effectiveness of various types of stability.

#### CRedit authorship contribution statement

**V. Vishnuvardhan Yadav:** Conceptualization, Methodology, Software, Formal analysis, Writing – original draft, Data curation. **B. Saravanan:** Conceptualization, Methodology, Validation, Investigation, Resources, Writing – review & editing, Visualization, Supervision, Project administration.

#### Declaration of competing interest

The authors declare that they have no known competing financial interests or personal relationships that could have appeared to influence the work reported in this paper.

#### Data availability

No data was used for the research described in the article.

#### References

- [1] M.K. Hossain, M.H. Ali, Transient stability augmentation of PV/DFIG/SG-based hybrid power system by nonlinear control-based variable resistive FCL, *IEEE Trans. Sustain. Energy* 6 (4) (2015) 1638–1649, <https://doi.org/10.1109/TSTE.2015.2463286>.
- [2] M.M.R. Singaravel, S.A. Daniel, MPPT with single DC-DC converter and inverter for grid-connected hybrid wind-driven PMSG-PV system, *IEEE Trans. Ind. Electron.* 62 (8) (2015) 4849–4857, <https://doi.org/10.1109/TIE.2015.2399277>.
- [3] H.M. Al-Masri, M. Ehsani, Feasibility investigation of a hybrid on-grid wind photovoltaic retrofitting system, *IEEE Trans. Ind. Appl.* 52 (3) (May 2016) 1979–1988, <https://doi.org/10.1109/TIA.2015.2513385>.
- [4] C. Wang, M.H. Nehrir, Power management of a stand-alone wind/photovoltaic/fuel cell energy system, *IEEE Trans. Energy Convers.* 23 (3) (2008) 957–967, <https://doi.org/10.1109/TEC.2007.914200>.
- [5] X. Li, D. Hui, X. Lai, Battery energy storage station (BESS)-based smoothing control of photovoltaic (PV) and wind power generation fluctuations, *IEEE Trans. Sustain. Energy* 4 (2) (2013) 464–473, <https://doi.org/10.1109/TSTE.2013.2247428>.
- [6] S.K. Ma, H. Geng, L. Liu, G. Yang, B.C. Pal, Grid-synchronization stability improvement of large scale wind farm during severe grid fault, *IEEE Trans. Power Syst.* 33 (1) (Jan. 2018) 216–226, <https://doi.org/10.1109/TPWRS.2017.2700050>.
- [7] U. Datta, A. Kalam, J. Shi, Battery energy storage system to stabilize transient voltage and frequency and enhance power export capability, *IEEE Trans. Power Syst.* 34 (3) (May 2019) 1845–1857, <https://doi.org/10.1109/TPWRS.2018.2879608>.
- [8] D. Abbes, A. Martinez, G. Champenois, Eco-design optimisation of an autonomous hybrid wind-photovoltaic system with battery storage, *IET Renew. Power Gener.* 6 (5) (Sep. 2012) 358–371, <https://doi.org/10.1049/iet-rpg.2011.0204>.
- [9] A.A. Eshkaftaki, A. Rabiee, A. Kargar, S.T. Boroujeni, An applicable method to improve transient and dynamic performance of power system equipped with DFIG-based wind turbines, *IEEE Trans. Power Syst.* 35 (3) (May 2020) 2351–2361, <https://doi.org/10.1109/TPWRS.2019.2954497>.
- [10] R. Yousefian, R. Bhattarai, S. Kamalasadani, Transient stability enhancement of power grid with integrated wide area control of wind farms and synchronous generators, *IEEE Trans. Power Syst.* 32 (6) (Nov. 2017) 4818–4831, <https://doi.org/10.1109/TPWRS.2017.2676138>.
- [11] G. Boukettaya, L. Krichen, A dynamic power management strategy of a grid connected hybrid generation system using wind, photovoltaic and flywheel energy storage system in residential applications, *Energy* 71 (2014) 148–159, <https://doi.org/10.1016/j.energy.2014.04.039>.
- [12] P. García, C.A. García, L.M. Fernández, F. Llorens, F. Jurado, ANFIS-based control of a grid-connected hybrid system integrating renewable energies, hydrogen and batteries, *IEEE Trans. Ind. Inform.* 10 (2) (2014) 1107–1117, <https://doi.org/10.1109/TII.2013.2290069>.
- [13] B. Liu, F. Zhuo, Y. Zhu, H. Yi, System operation and energy management of a renewable energy-based DC micro-grid for high penetration depth application, *IEEE Trans. Smart Grid* 6 (3) (2015) 1147–1155, <https://doi.org/10.1109/TSG.2014.2374163>.
- [14] A.Z. al Shaqsi, K. Sopian, A. Al-Hinai, Review of energy storage services, applications, limitations, and benefits, *Energy Rep.* 6 (2020) 288–306, <https://doi.org/10.1016/j.egy.2020.07.028>.
- [15] P. Mukherjee, V.v. Rao, Superconducting magnetic energy storage for stabilizing grid integrated with wind power generation systems, *J. Mod. Power Syst. Clean Energy* 7 (2) (2019) 400–411, <https://doi.org/10.1007/s40565-018-0460-y>.
- [16] E.M. Molla, C.C. Kuo, Voltage sag enhancement of grid connected hybrid PV-wind power system using battery and SMES based dynamic voltage restorer, *IEEE Access* 8 (2020) 130003–130013, <https://doi.org/10.1109/ACCESS.2020.3009420>.
- [17] Z. Zheng, X. Xiao, C. Huang, C. Li, Enhancing transient voltage quality in a distribution power system with SMES-based DVR and SFCL, *IEEE Trans. Appl. Supercond.* 29 (2) (2019) 2–6, <https://doi.org/10.1109/TASC.2018.2882469>.
- [18] A.M. Gee, F. Robinson, W. Yuan, A superconducting magnetic energy storage-Emulator/Battery supported dynamic voltage restorer, *IEEE Trans. Energy Convers.* 32 (1) (2017) 55–64, <https://doi.org/10.1109/TEC.2016.2609403>.
- [19] G. Li, Y. Chen, A. Luo, H. Wang, An enhancing grid stiffness control strategy of STATCOM/BESS for damping sub-synchronous resonance in wind farm connected to weak grid, *IEEE Trans. Ind. Inform.* 16 (9) (2020) 5835–5845, <https://doi.org/10.1109/TII.2019.2960863>.
- [20] L. Wang, et al., Damping of subsynchronous resonance in a hybrid system with a steam-turbine generator and an offshore wind farm using a unified power-flow controller, *IEEE Trans. Ind. Appl.* 57 (1) (2021) 110–120, <https://doi.org/10.1109/TIA.2020.3032934>.
- [21] A.M. Shiddiq Yunus, A. Abu-Siada, M.I. Mosaad, H. Albalawi, M. Aljohani, J.X. Jin, Application of SMES technology in improving the performance of a DFIG-WECS connected to a weak grid, *IEEE Access* 9 (2021) 124541–124548, <https://doi.org/10.1109/ACCESS.2021.3110995>.
- [22] H. Peng, L. Luan, Z. Xu, W. Mo, Y. Wang, Event-triggered mechanism based control method of SMES to improve microgrids stability under extreme conditions, *IEEE Trans. Appl. Supercond.* 31 (8) (2021) 8–11, <https://doi.org/10.1109/TASC.2021.3090379>.
- [23] A. M and S. M, in: HVDC Tielink Based Load Frequency Control Coordinated With SMES And TCSC, 2022, pp. 1–6, <https://doi.org/10.1109/icfer54831.2022.9893664>.
- [24] S.M. Said, M. Aly, H. Balint, An efficient reactive power dispatch method for hybrid photovoltaic and superconducting magnetic energy storage inverters in utility grids, *IEEE Access* 8 (2020) 183708–183721, <https://doi.org/10.1109/ACCESS.2020.3029326>.
- [25] J. Liu, M. Yang, W. Tao, in: Impedance-based stability analysis of grid-tied photovoltaic system with superconducting magnetic energy storage system 31(8), 2021, pp. 8–11.
- [26] S. Nomura, T. Nitta, T. Shintomi, Mobile superconducting magnetic energy storage for on-site estimations of electric power system stability, *IEEE Trans. Appl. Supercond.* 30 (4) (Jun. 2020), <https://doi.org/10.1109/TASC.2020.2982877>.
- [27] T.L. Zhang, Q. Zhou, S. Mu, H. Li, Y.J. Li, J. Wang, Voltage-based segmented control of superconducting magnetic energy storage for transient power fluctuation suppression in island DC microgrid, *IEEE Trans. Appl. Supercond.* 31 (8) (Nov. 2021), <https://doi.org/10.1109/TASC.2021.3101760>.
- [28] L. Wang, Q.S. Vo, A.v. Prokhorov, Stability improvement of a multimachine power system connected with a large-scale hybrid wind-photovoltaic farm using a supercapacitor, in: 2017 IEEE/IAS 53rd Industrial and Commercial Power Systems Technical Conference, I and CPS 2017, Jun. 2017, <https://doi.org/10.1109/ICPS.2017.7945117>.
- [29] A. Adamczyk, M. Altin, Ö. Göksu, R. Teodorescu, F. Iov, Generic 12-bus test system for wind power integration studies, in: EPE Joint Wind Energy And T And D Chapters Seminar, 2012, pp. 1–6.
- [30] J. Hossain, A. Mahmud, Green energy and technology large scale renewable power generation advances in technologies for generation, transmission and storage [Online]. Available, <http://www.springer.com/series/8059>.
- [31] M.E. Haque, M. Negnevitsky, K.M. Muttaqi, A novel control strategy for a variable-speed wind turbine with a permanent-magnet synchronous generator, *IEEE Trans. Ind. Appl.* 46 (1) (2010) 331–339, <https://doi.org/10.1109/TIA.2009.2036550>.
- [32] Wind energy conversion systems, in: Grid Integration of Wind Energy, John Wiley & Sons, Ltd, 2014, pp. 31–117, <https://doi.org/10.1002/9781118703274.ch2>.
- [33] D. Zhou, F. Blaabjerg, T. Franke, M. Tønnes, M. Lau, Comparison of wind power converter reliability with low-speed and medium-speed permanent-magnet

- synchronous generators, *IEEE Trans. Ind. Electron.* 62 (10) (2015) 6575–6584, <https://doi.org/10.1109/TIE.2015.2447502>.
- [34] A. Chikh, A. Chandra, An optimal maximum power point tracking algorithm for PV systems with climatic parameters estimation, *IEEE Trans. Sustain. Energy* 6 (2) (2015) 644–652, <https://doi.org/10.1109/TSTE.2015.2403845>.
- [35] M.G. Villalva, J.R. Gazoli, E.Ruppert Filho, Modeling and circuit-based simulation of photovoltaic arrays, in: 2009 Brazilian Power Electronics Conference, COBEP2009, 2009, pp. 1244–1254, <https://doi.org/10.1109/COBEP.2009.5347680>.
- [36] M.G. Villalva, J.R. Gazoli, E.R. Filho, Comprehensive approach to modeling and simulation of photovoltaic arrays, *IEEE Trans. Power Electron.* 24 (5) (2009) 1198–1208, <https://doi.org/10.1109/TPEL.2009.2013862>.
- [37] L. Wang, Q.S. Vo, A.v. Prokhorov, Dynamic stability analysis of a hybrid wave and photovoltaic power generation system integrated into a distribution power grid, *IEEE Trans. Sustain. Energy* 8 (1) (2017) 404–413, <https://doi.org/10.1109/TSTE.2016.2602370>.
- [38] N.Ghardash Khani, Improving dynamic response of PEMFC using SMES and bidirectional DC/DC converter, *Automatika* 63 (4) (2022) 745–755, <https://doi.org/10.1080/00051144.2022.2066768>.
- [39] L.N. Khanh, J.J. Seo, Y.S. Kim, D.J. Won, Power-management strategies for a grid-connected PV-FC hybrid system, *IEEE Trans. Power Deliv.* 25 (3) (2010) 1874–1882, <https://doi.org/10.1109/TPWRD.2010.2047735>.
- [40] D. Sera, L. Mathe, T. Kerekes, S.V. Spataru, R. Teodorescu, On the perturb-and-observe and incremental conductance mppt methods for PV systems, *IEEE J. Photovoltaics* 3 (3) (2013) 1070–1078, <https://doi.org/10.1109/JPHOTOV.2013.2261118>.
- [41] Venkata Yaramasu, Bin Wu, *Model Predictive Control of Wind Energy Conversion Systems*, Second ed., John Wiley & Sons, 2017.
- [42] L. Wang, Q.S. Vo, A.V. Prokhorov, Stability improvement of a multimachine power system connected with a large-scale hybrid wind-photovoltaic farm using a supercapacitor, *IEEE Trans. Ind. Appl.* 54 (1) (2018) 50–60, <https://doi.org/10.1109/TIA.2017.2751004>.